The non-linear impact of El Niño, La Niña and the Southern Oscillation on seasonal and regional Australian precipitation

Article *in* Journal of Southern Hemisphere Earth System Science · May 2017

DOI: 10.22499/3.6701.003

CITATIONS
14

READS
457

2 authors:

Christine T. Y. Chung
Bureau of Meteorology
121 PUBLICATIONS **8,183** CITATIONS

SEE PROFILE

Scott Power
Bureau of Meteorology
129 PUBLICATIONS **9,307** CITATIONS

SEE PROFILE

Chung. *Journal of Southern Hemisphere Earth Systems Science* (2017) 67:1, 25-45 DOI: 10.22499/3.6701.003

The non-linear impact of El Niño, La Niña and the Southern Oscillation on seasonal and regional Australian precipitation

Christine T. Y. Chung[1] and Scott B. Power[1]

[1] Bureau of Meteorology, Australia

(Manuscript received October 2016; accepted February 2017)

The relationship between El Niño-Southern Oscillation (ENSO) indices and precipitation (P) in some parts of Australia has previously been shown to be non-linear on annual and seasonal time scales. Here we examine the relationship between P and the Southern Oscillation Index (SOI) at all Australian locations and in all seasons. We show that in many Australian regions, there is more-than-expected P during strong La Niña years (SOI>13), but less-than-expected drying during strong El Niño years (SOI<-13). Statistically significant non-linearities are found over northern NT, QLD and parts of WA during SON, and parts of QLD, NSW, and VIC during DJF, when regressing P against June-December SOI. During the MAM immediately preceding a June-December ENSO year, and during JJA, the rainfall-SOI relationship is linear over most of the country. Systematic eastward shifts in P patterns can explain non-linearities over northern Australia, but do not explain non-linearities southward of approximately 20˚S. The seasonal P distribution is decomposed into FP, the fraction of days on which P falls, and PD, the amount of rain per day on days when P is non-zero. Both FP and PD display a non-linear relationship with SOI similar to the P-SOI relationship, although the relative influence of each term on P is spatially and seasonally dependent.

1 Introduction

Australian rainfall is strongly influenced by the El Niño-Southern Oscillation (ENSO; McBride and Nicholls 1983; Ropelewski and Halpert 1987; Allan 1988; Nicholls et al. 1997; Power et al. 1998; Power et al. 1999; Power et al. 2006; Risbey et al. 2009). Risbey et al. (2009) showed that the Southern Oscillation Index (SOI), which measures the amplitude and type of ENSO event, is highly correlated with rainfall over most parts of Australia. The correlations vary seasonally, and are most widespread between June – December. Generally, during El Niño (La Niña) events, when the central and eastern equatorial Pacific sea surface temperatures (SSTs) warm (cool), there tends to be less (more) rainfall over Australia. However, this relationship has been shown to be non-linear (Power et al. 2006; Lim et al. 2009; Cai et al. 2010; Cai et al. 2011; Cai et al. 2012; King et al. 2013; King et al. 2015). Power et al. (2006) showed that there is a non-linear relationship between the SOI and the all-Australia annual rainfall, with a large La Niña (LN) event producing a stronger rainfall response than an El Niño (EN) event of a similar magnitude. They showed that Australia tends to dry out during EN events, but the degree of drying is not as tightly linked to the magnitude of the SOI anomaly. They raised the possibility that the non-linearity arises from either (i) an eastward shift in the rainfall away from the continent during large EN events resulting in a weaker rainfall response over Australia or (ii) from the non-negative nature of rainfall. Cai et al. (2010) investigated non-linearity in December-January-February (DJF) rainfall over southeast Queensland (QLD) and attributed it to the eastward shift of Pacific Ocean SST anomalies, away from Australia during EN events. King et al. (2013) identified a significant correlation between the strength of La Niña events and extreme rainfall intensity during October-March over southeast Australia, but none for El Niño events, suggesting that this is due to enhancements in near-surface moisture flux convergence during strong La Niña years.

Corresponding author: Christine T. Y. Chung, Bureau of Meteorology, Melbourne
Email: christine.chung@bom.gov.au

In other parts of the world, ENSO also produces a non-linear rainfall response (e.g., Hoerling et al. 1997; Power et al. 2013; Frauen and Dommenget 2014; Chung et al. 2014; Sun et al. 2015). The EN-LN asymmetry has been shown to affect the rainfall distribution over North America, particularly for strong events (Hoerling et al. 1997; Power et al. 2006), Papua New Guinea (Smith et al. 2013), several tropical Pacific island nations (Murphy et al. 2014) and New Zealand (Mullan 2008). Differences in the location of the Pacific SST anomalies during EN events also produce significantly different temperature and precipitation anomalies over North America and the North Atlantic (Hu et al. 2012). Atmospheric general circulation model experiments using prescribed SSTs have also shown that linearly varying the magnitude of an EN event produces a large non-linear precipitation increase over the equatorial Pacific Ocean and an eastward shift of the rainfall patterns along the equator (Chung et al. 2014; Power et al. 2013). This non-linearity also occurs to a lesser degree for LN events, with drying and a westward shift of rainfall patterns along the equatorial Pacific (Chung and Power 2014).

On average, Australia experiences more rainfall during LN years and less during EN years. However, it is a generalisation to assume that all strong EN years bring about droughts while strong LN years bring about floods over the Australian region. While LN years can be expected to generate a large positive rainfall anomaly in many regions in Australia (e.g., Hendon et al. 2013), equivalently strong EN events may not bring about a large negative rainfall anomaly (e.g., Wang and Hendon 2007). In fact, in some regions, more rainfall may occur during strong El Niño years than during other years. A study of this non-linearity using CMIP5 climate model output found that thermodynamic processes play a larger role in ENSO-related rainfall non-linearity than dynamic processes (King et al. 2015).

While previous observation-based work has focused only on single regions and seasons, or an all-Australia average, in this paper we analyse gridded data spanning the whole country for all seasons, and we quantify the rainfall-SOI relationship in all regions. We will address the following questions: i) Where and when is the rainfall-SOI relationship over Australia non-linear? ii) What is the statistical nature and magnitude of the non-linearity? iii) What features of the daily rainfall distribution in these areas cause or contribute to the non-linearity? iv) To what extent does a large-scale systematic shift in rainfall over or around Australia during ENSO events contribute to the non-linearity evident?

The data used in this investigation is described in Section 2. The rainfall-SOI relationship over Australia is examined in detail in Section 3. In Section 4, the non-linearity in the rainfall-SOI relationship is examined for each season. The rainfall-SOI relationship in specific regions where marked non-linearity is evident is examined in detail. In Section 5, we present the rainfall patterns over Australia and the Pacific for ENSO events of varying strengths, and we compare the spatial patterns of rainfall anomalies during EN and LN events to assess the extent to which the anomalies arise from systematic large-scale shifts. The results are summarised and briefly discussed in Section 6.

2 Data and Methods

In the sections 'The rainfall-SOI relationship over Australia', 'Non-linearity in total seasonal precipitation and decomposition of daily precipitation distributions', we analyse the Australian Water Availability Project (AWAP) data set on an 0.25˚ x0.25˚ grid (Jones et al. 2004, 2009) over the period 1910-2012. As AWAP was created by interpolating station data, there may be biases in the rainfall data from remote regions with relatively few stations (e.g., King et al 2013). Based on the Bureau of Meteorology's rainfall station map (http://www.bom.gov.au/climate/data/), we therefore mask out two regions with limited coverage. The first covers the eastern part of Western Australia (WA), the southwestern part of the Northern Territory (NT), and the western part of South Australia (SA) (121˚E-134˚E, 18˚S-34˚S) and the second covers northeastern SA and the southeastern part of NT (136˚E-139˚E, 23˚S-29˚S).

In the sections 'Non-linear response to ENSO' and 'Large-scale shifts', we analyse monthly mean data from the Global Precipitation Climatology Project (GPCP; Adler et al. 2003) which consists of monthly data on a global 2.5˚x2.5˚ grid spanning 1979-2009. Throughout the manuscript, we use the June to December SOI average to classify ENSO events, with EN events having SOI < -5 and LN events having SOI > 5 (e.g., Salinger et al. 2014; Power and Smith 2007; Power et al. 2006). SOI values are obtained from the Australian Bureau of Meteorology. (ftp://ftp.bom.gov.au/anon/home/ncc/www/sco/soi/soiplaintext.html).

Throughout the analysis, statistical significance is determined in one of two ways. Firstly, t-values are used to calculate the significance of correlation coefficients and non-linearity. For non-linearity, the difference between two linear regression coefficients (i.e. for SOI < 0 and SOI > 0 years) is calculated and a one-tailed t-test is performed to check if the two coefficients are significantly different. Secondly, the significance of observed anomalies is estimated using a Monte Carlo meth-

od. At each grid point, the observed anomalies are randomised by generating random SOI values (1000 trials are conducted). For a particular SOI bin, any location in which the magnitude of the observed rainfall anomalies exceeds the randomised anomalies in more than 95 per cent of the trials is deemed to have significant non-linearity.

3 The rainfall-SOI relationship over Australia

In this section we will further analyse the relationship between Australian rainfall and the SOI using seasonal means of AWAP data. In each ENSO year, JJA, SON, and the DJF beginning in that calendar year are all classified as belonging to that ENSO year. Analysis is conducted on the MAM immediately after the ENSO year (MAM+1) and the MAM that falls immediately prior to the JJA in the ENSO year (MAM-1), to see if they exhibit any early or late ENSO signals.

We will first evaluate the ability of a linear model to describe the rainfall-SOI relationship. As we will see, there are limitations to using a linear model to describe the rainfall-SOI relationship for all years, especially in areas that experience very low or high rainfall. For example, in regions where the rainfall-SOI relationship is non-linear, a linear fit to the data sometimes underestimates the amount of rainfall received and predicts negative rainfall values. The model can be improved by fitting separate linear models to SOI < 0 and SOI > 0 instead, and the difference in the linear regression coefficients can provide a measure of the degree of non-linearity. A similar approach (using Niño3.4 and other indices instead of SOI) has been used to point out the existence of a non-linear rainfall response to ENSO events in southeast QLD during DJF (Cai et al. 2010), and an asymmetry between ENSO and Indian Ocean Dipole events during SON (Cai et al 2012). Risbey et al. (2009) noted that SOI provides a higher correlation with rainfall than the SST-based NIÑO indices, although there is some multidecadal variability (e.g., Power et al. 1999; Arblaster et al. 2002; see discussion in 'Conclusion').

We first examine rainfall-SOI lines-of-best-fit for (i) all years (1901-2012), (ii) all SOI<0 years, and (iii) all SOI>0 years separately. Fig 1 shows scatter plots of the all-Australian seasonally-averaged rainfall for all five periods. We linearly regress rainfall against SOI<0 years (with the slope, S_{EN}, and lines of best-fit depicted using red lines), all SOI>0 years (with the slope, S_{LN}, in blue lines), and all years (with the slope, SALL, grey lines). In two seasons (JJA and SON) the non-linearity, measured as the difference between S_{LN} and S_{EN}, is significant at the five per cent level as indicated by the p-values in the figures. In DJF and MAM+1, the non-linearity is significant at the ten per cent level. During MAM-1, the rainfall-SOI relationship is approximately linear.

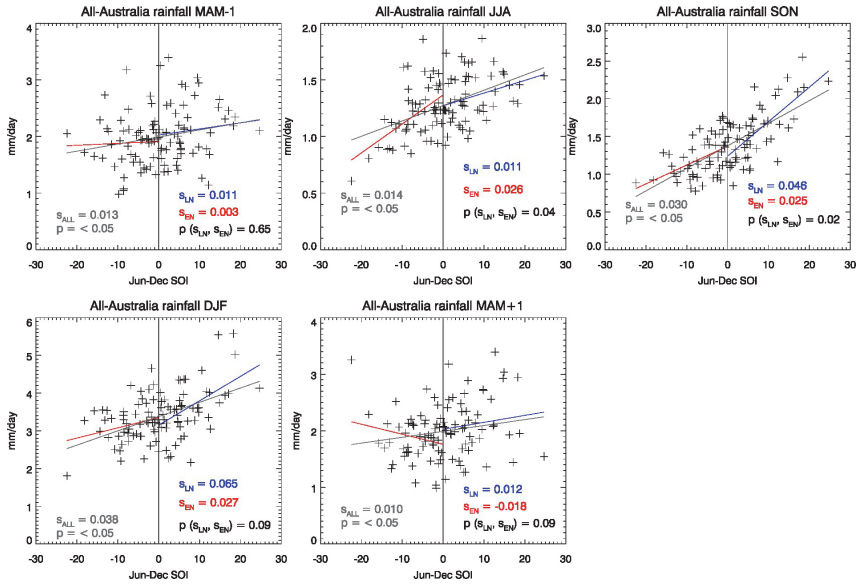

Figure 1 Scatter plots showing AWAP seasonal all-Australian averaged precipitation as a function of Jun-Dec SOI (1910-2012). The linear fits to negative, positive, and all SOI values are shown as red, blue, and grey lines respectively. coefficients (s_{EN}, s_{LN}, and s_{ALL}), and p-values indicating the significance of the linear fit (s_{ALL}) and significance of the difference between s_{LN} and s_{EN}, (p(s_{LN}, s_{EN})) are shown in coloured text. Note in this figure, SOI for a particular Jun-Dec (year 0) corresponds to the seasons MAM-1 (year 0), D(year 0)JF(year 1), and MAM+1 (year 1).

3.1 The rainfall-SOI relationship for all years

In this section we examine the spatial distribution of the rainfall-SOI relationship. The correlation coefficient, SALL, between rainfall and the SOI is computed for 1910-2012 and shown in Fig 2, with the maps stippled where SALL is significant. Significance is calculated at the five per cent level using a one-tailed t-test. It is interesting to note that there are statistically significant relationships in at least one season, in all parts of Australia that are considered in this study. Previous studies have shown that the impact of ENSO on Australian rainfall is most widespread during SON (Risbey et al. 2009). The correlation is strongest and most widespread in SON and DJF, over north and east Australia. During MAM-1, SALL is significant in western WA and parts of Victoria (VIC) and QLD. During JJA, SALL is significant over most of eastern Australia, western New South Wales (NSW), and eastern SA. The correlation is weakest during MAM+1, with only the Cape York region and small parts of the NT, SA, and NSW displaying a significant correlation. Over most northern Tasmania, the rainfall-SOI relationship is significant during JJA and SON.

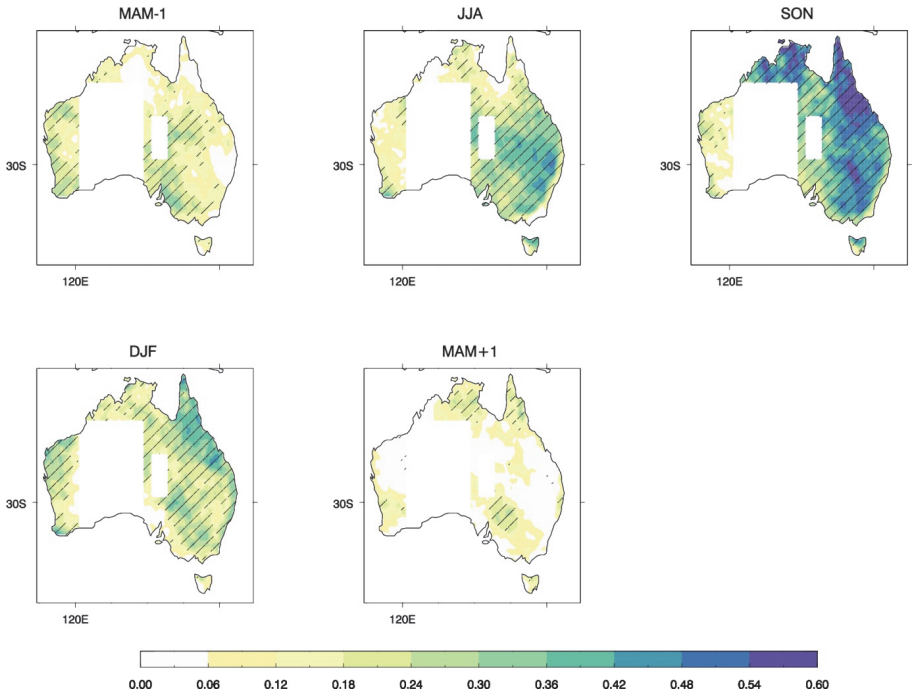

Figure 2 Correlation coefficients for AWAP monthly precipitation and June-Dec SOI (1910-2012) for MAM-1 (the season immediately preceding the June-Dec used to calculate the SOI), JJA, and SON, DJF, and MAM+1 (the season following the SOI year). Stippling indicates five per cent significance.

3.2 Map significance and seasonal coverage of non-linearity

Although large areas of the country have a statistically significant correlation with the SOI in all seasons, the observed rainfall in many areas deviates from a purely linear fit. In this section we examine the spatial extent of non-linearity in the relationship between rainfall and the SOI more carefully. As it is possible by chance to obtain statistical significance in some locations over the grid, we also determine the statistical significance of the areal extent of non-linearity, considering only the non-masked regions of study. Non-linearity is calculated by fitting a linear model to the SOI>0 and SOI<0 years separately as in Fig 1, and is deemed to be significant where the difference in the regression coefficients for SOI>0 and SOI<0 years, Δs, is significant at the five per cent level using a one-sided t-test, as outlined in 'Data and Methods'. For each season, Δs is statistically significant over 6.2% (MAM-1), 3.2% (JJA), 18.1% (SON), 12.8% (DJF), and 10.7% (MAM+1) of the total non-masked study area.

We then test the overall significance of the area covered by Δs (see Appendix). Using a Monte Carlo approach (Livezey and Chen 1983; Power and Mysak 1992), we find that only the non-linearities occurring in SON, DJF, and MAM+1 cover a large enough area to be significant at the five per cent level. We henceforth focus on these three seasons only.

In Figs 3-5 we plot for SON, DJF, and MAM+1 the anomalies for observed rainfall (left columns), a purely linear fit (middle columns), and the difference between observed and linear-fit anomalies (right columns). Anomalies are calculated with respect to the 1910-2012 climatology for each season. The analysis is shown for two SOI bins: (i) strong EN (SOI < -13, panels a-c) and (ii) strong LN (SOI > 13, panels d-f). Note that while analyses were also conducted using all years, plots are only provided for strong EN and strong LN years to simplify presentation. For the observed anomalies in the left columns, significance is calculated using the Monte Carlo method outlined in 'Data and Methods'. For the anomalies (or deviations) from the linear fit in the middle columns, the plots are stippled where the rainfall-SOI correlation is significant, as in Fig 2. In the right columns, the maps are stippled where the non-linearity (i.e. the difference between SOI>0 and SOI<0 regression coefficients) is significant at the five per cent level. We will now examine this analysis of non-linearity in each season.

i) SON

Fig 3 shows maps for SON, where the observed anomalies (Figs 3a, d) are largest over eastern Australia, especially during strong LN years. As expected, the composite of strong EN years exhibits drying over most of the country, while the composite of strong LN years exhibits an increase in precipitation. While both observed and linear-fit anomalies are negative over eastern Australia during strong EN years (Figs 3a, b), the observed anomalies are smaller than those from the linear fit over most of QLD, the Kimberley region in northern Australia, and western WA. During strong LN years, the observed and linear-fit anomalies are similar (Figs 3d, e), though the observed anomalies are larger over the same regions.

The rightmost column (Figs 3c, f) highlights the difference between the observed and linear-fit anomalies. During strong EN years, the observed rainfall does not dry as much as predicted by the linear model over northern, western, and eastern Australia, indicating that the reduction in rainfall over these regions tends to be less severe than expected assuming a linear rainfall-SOI relationship. During strong LN years, the observed rainfall is instead larger than that predicted by the linear model over the same regions. Therefore, assuming a linear rainfall-SOI relationship would underestimate the amount of rainfall during strong LN years and strong EN years over much of Australia.

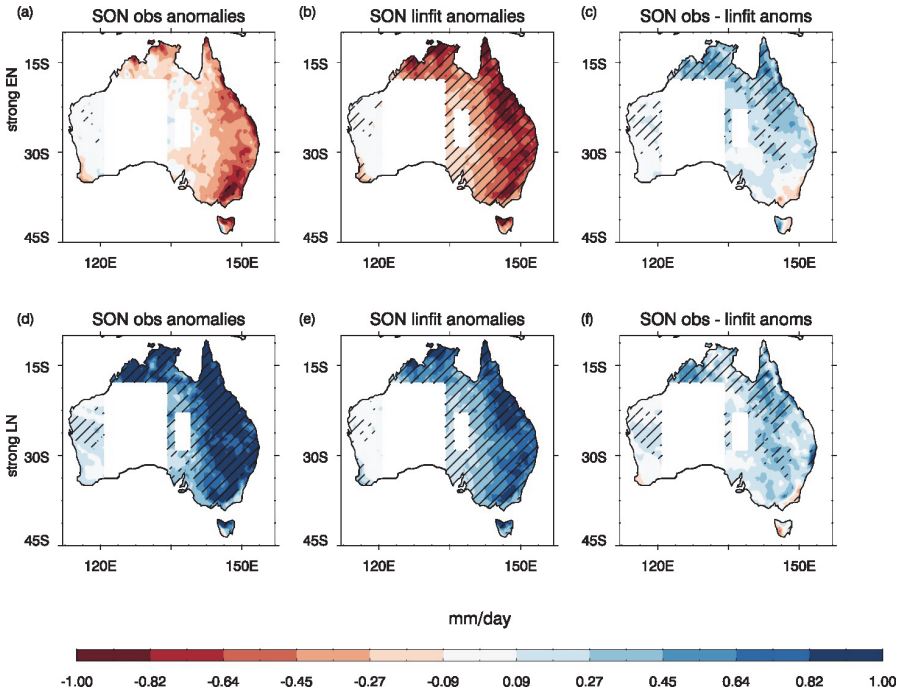

Figure 3 Precipitation anomalies for SON for (left) observed precipitation, and (middle) linear fit to the data, and (right) the difference between observed and linear fit anomalies corresponding to strong EN (top) and strong LN (bottom) years respectively. In the left panels, stippling shows where observed anomalies are significant using a Monte Carlo method. In the middle panels, stippling shows where the correlation coefficient is significant, as in Fig 2. In the right panels, areas where a non-linear relationship is significant are stippled. All significance is calculated at the five per cent level. Anomalies are calculated with respect to the 1910-2012 climatology.

ii) DJF

Fig 4 shows maps for DJF, where the observed rainfall anomalies are largest over north and east Australia. During strong EN years (Figs 4a, d), the observational composite shows a strong negative (dry) anomaly over most of QLD, but interestingly, a positive (wet) anomaly in the eastern inland, parts of WA, and the Kimberley region. However, very few regions show statistically significant rainfall anomalies during strong EN years, indicating that the largest five per cent of negative rainfall anomalies do not occur during strong EN years. The linear fit to the data produces negative anomalies over the whole country, with the largest anomalies over northern Australia and along the east coast.

During strong LN years (Figs 4d-f), both observed and linear-fit anomalies show an increase in rainfall over north and eastern Australia, although the observed anomalies are larger over most regions. The observed rainfall anomalies over a small part of northeastern Australia are statistically significant. As with SON, a purely linear fit underestimates the amount of rainfall during strong EN years and strong LN years over most of eastern Australia and parts of the north.

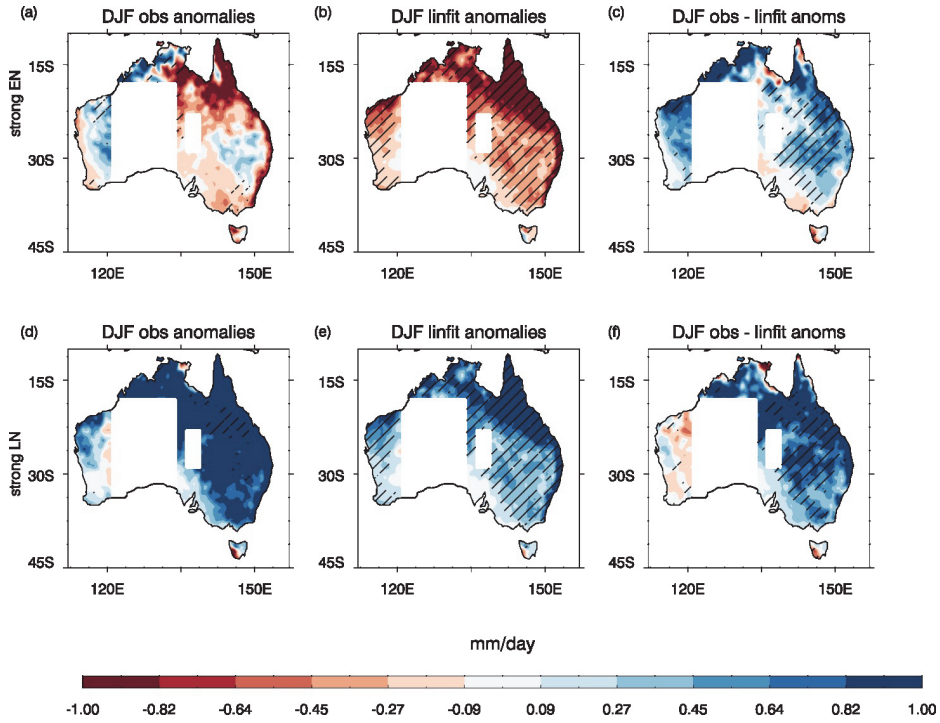

Figure 4 As in Fig 3, but for DJF.

iii) MAM+1

During MAM+1, there is only a weak correlation between rainfall and the SOI in parts of northern and southeastern Australia as shown in Fig 2. Fig 5a shows a positive rainfall anomaly over inland regions of the NT and QLD during strong EN years, which is in contrast from what is expected from a linear fit (Fig 5b). During strong LN years, a positive anomaly is observed in northern QLD, and a negative anomaly is observed over western WA (Fig 5d). Over far northern Australia, there is generally less rainfall than is predicted by a linear fit, and over southeastern Australia, there is more rainfall than predicted by a linear fit.

In summary, these maps indicate that during SON and DJF, over several regions, there is a non-linear relationship between rainfall and SOI which results in a larger-than-expected amount of rainfall during strong LN years and less-than-expected drying during strong EN years. During MAM+1, when the SOI only exerts a weak influence on the rainfall, the nature of the non-linearity is different over most of the country, but particularly over the NT and QLD, with large positive rainfall anomalies during strong EN years and negative rainfall anomalies during strong LN years. In all these cases, a simple least-squares linear fit applied to all years does not adequately describe the rainfall-SOI relationship.

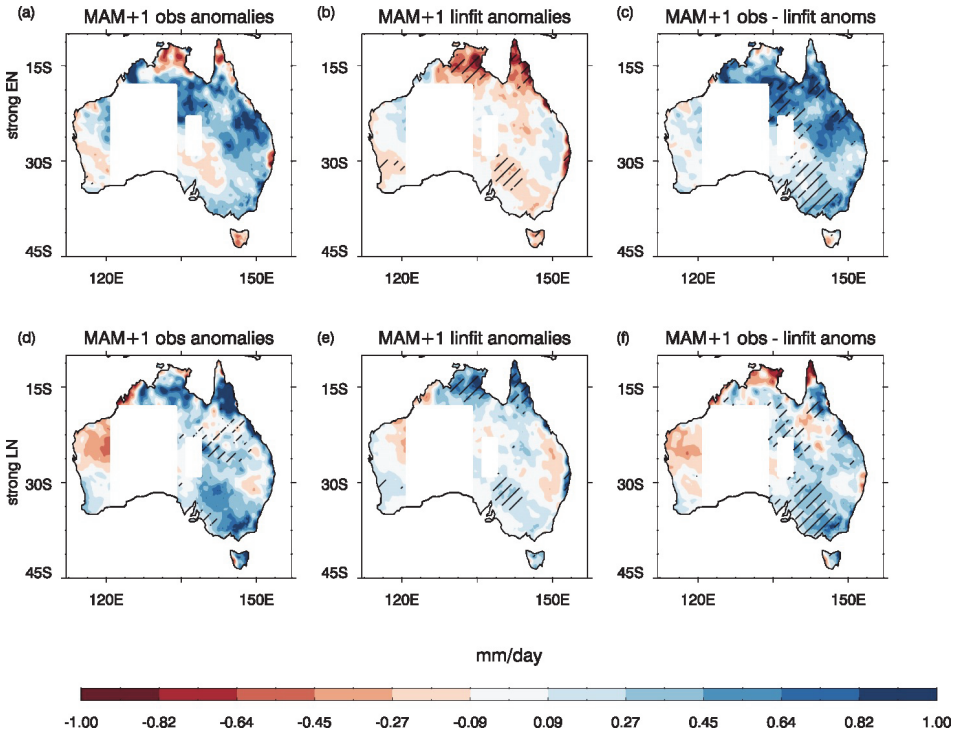

Figure 5 As in Fig 3, but for MAM+1 (the MAM season directly following the June-December used in the SOI average).

3.3 The rainfall-SOI relationship within EN and LN years

In the previous section we examined non-linearity arising from comparing the linear fits to all EN years to the linear fits to all LN years. We saw that in some regions and seasons the rainfall response per unit change in the SOI during LN years was different to the rainfall response per unit change in the SOI during EN years. It is possible, however, that non-linearity arises within EN or LN years themselves. For example, it might be that large positive excursions in the SOI are associated with a disproportionately large rainfall response in comparison to the rainfall response during weak positive excursions in the SOI. Similarly, it might be that in some regions large negative excursions in the SOI are associated with disproportionately small rainfall declines, in comparison to weaker negative excursions in the SOIs. We now test whether such non-linearity exists.

Figures 6-8 show seasonal rainfall anomalies from observations (left columns), a linear fit to only EN/LN years (middle columns), and the difference between observations and the linear fit (right columns) for SON, DJF, and MAM+1. The top two rows (panels a-f) correspond to strong and weak negative excursions in the SOI, labelled strong EN (SOI<-13) and weak EN (-13<SOI<-5). The bottom two rows (panels g-l) correspond to weak and strong positive excursions in the SOI, labelled strong LN (SOI>13) and weak LN (5<SOI<13). Note that the Australian Bureau of Meteorology uses a similar SOI scale when classifying the strength of events, in conjunction with other factors such as SSTs and Australian precipitation patterns. Unlike the analysis from the previous section, the linear fit is performed for EN and LN years separately. In the left and middle columns, stippling indicates where the correlation between rainfall and SOI is significant at the five per cent level. The rightmost columns show the difference between the observed and linear-fit anomalies. To identify regions in which non-linearities within EN and LN years are significant, we compare the slopes of the lines-of-best-fit connecting the mean rainfall in each SOI bin. Specifically, we ask, is the mean rainfall difference between neutral and weak positive/negative excursion years ($\Delta P1$) significantly different from the rainfall difference between weak and strong SOI excursion years ($\Delta P2$)? If the value of $\Delta P1$ does not overlap with $\Delta P2 \pm SE2$ (where SE is 1.96 times the standard error of ΔP), and vice versa, the rainfall-SOI relationship is deemed to be significantly non-linear.

i) SON

Over most of eastern Australia, the SON rainfall-SOI correlation is significant during EN years (Figs 6a-f). Comparing the observed and linear-fit anomalies, parts of the NT and most of QLD show significant non-linearity during EN years (Figs 6c, f). In these regions, the linear fit underestimates the amount of rainfall received during strong EN years.

During LN years (Figs 6g-l), the rainfall-SOI correlation is significant over most of the country. Small regions of significant non-linearity are found in parts of inland QLD and NSW, where the linear fit overestimates the amount of rainfall during weak LN years and underestimates it during strong LN years (Figs 6i, l).

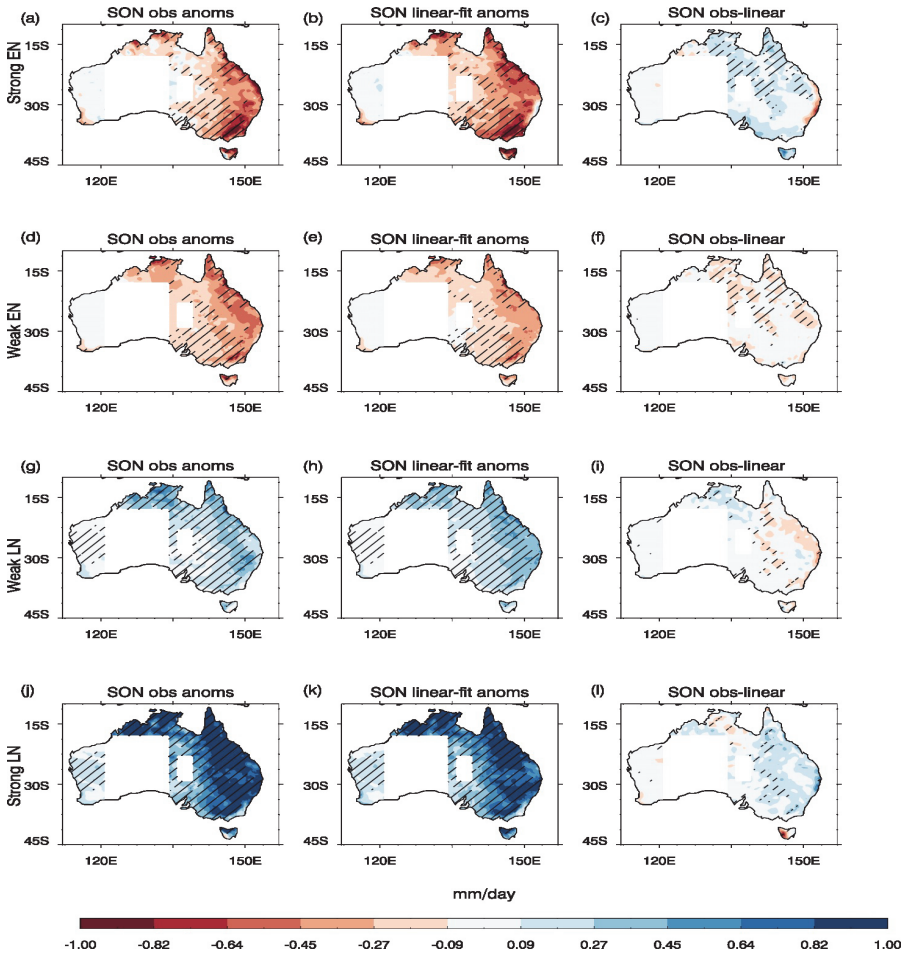

Figure 6 Linearity within EN/LN years separately using June-December SOI. SON anomalies for (a,d) observed rainfall, (b,e) linear fit to the data for EN years only, and (c,f) the difference between observed and linear fits to the data for EN years only. (g-l): The same, but for LN years only. Stippling in the left and middle columns indicates where linear regression coefficients for EN/LN years are significant at the five per cent level. Stippling in the right column indicates non-linearity within EN/LN years (see text for details on calculation). Anomalies are calculated with respect to the 1910-2012 climatology.

ii) DJF

The correlation between DJF rainfall and SOI during EN years is examined in Figs 7a-f. The observed anomalies for strong and weak EN years (Figs 7a, d) show that even though most of the country is drier than average during strong EN years, there is very little statistically significant correlation between rainfall and SOI for EN years. This indicates that a strong negative excursion in the SOI is not necessarily linked to more drying than a weak negative excursion event over

most of the country. In fact, over most of inland NSW, southern QLD, and WA, strong EN years show a positive rainfall anomaly.

Figs 7c and 7f show the differences between observed and linear-fit anomalies. Both sets of anomalies differ most over the northern NT and QLD, with more-than-expected drying during weak EN years, and less-than-expected drying during strong EN years. Figs 7c, f are stippled over parts of WA and southeastern Australia, where ΔP1 (the mean rainfall difference between SOI≈0 and weak EN bins) and ΔP2 (the mean rainfall difference between weak EN and strong EN bins), are significantly different, i.e. exhibiting non-linearity within EN events.

During LN years (Figs 7g-l), there is a significant correlation between SOI and rainfall over northern and eastern Australia: rainfall anomalies increase as the SOI increases (Figs 7g, j). The observed (Figs 7g, j) and linear-fit anomalies (Figs 7h, k) match reasonably well over most of the country, with the largest differences occurring over northern Australia and along the east coast, where the linear fit underestimates the amount of rainfall received in strong LN events and overestimates the rainfall in weak LN events. Regions along the northeast coast of QLD and northern NT display significant non-linearity (Figs 7i, l).

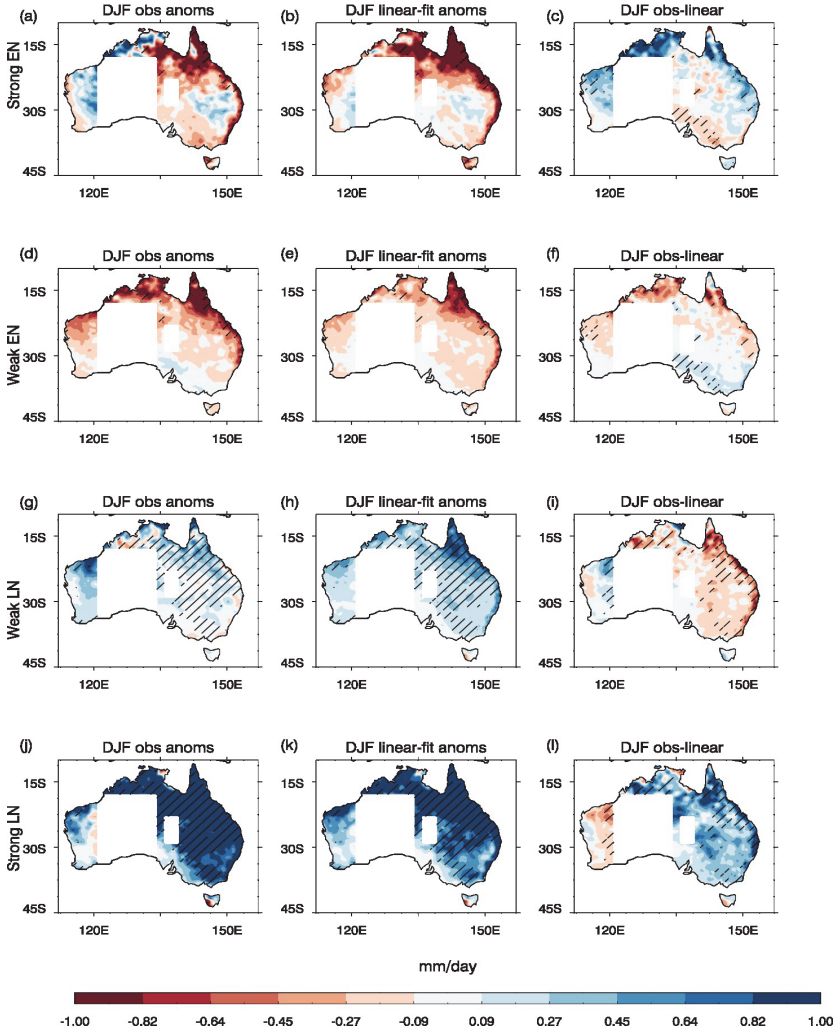

Figure 7 As in Fig 6, but for DJF.

iii) MAM+1

Fig 8 corresponds to MAM+1, where there is no significant rainfall-SOI correlation during EN years (Figs 8a, d). Weak EN years exhibit drying over northern and eastern Australia, but strong EN years exhibit a large positive rainfall anomaly. The linear fit for EN years has a negative slope over this region which underestimates the amount of rainfall received during strong EN years and overestimates the rainfall during weak EN years across the inland NT, and most of NSW (Figs 8c, f). In these regions, the non-linearity is found to be significant.

During LN years in MAM+1 (Fig 8g-l), the rainfall-SOI correlation is significant in VIC, and around the SA/NSW/QLD border. For weak LN years, the observations match the linear fit relatively well, whereas for strong LN years, there is a larger difference over western WA, and parts of south QLD, where there is a significant non-linearity (Figs 8i, l). In south QLD, the observations show drying during strong LN years (Fig 8j), in contrast to the linear fit (Fig 8k).

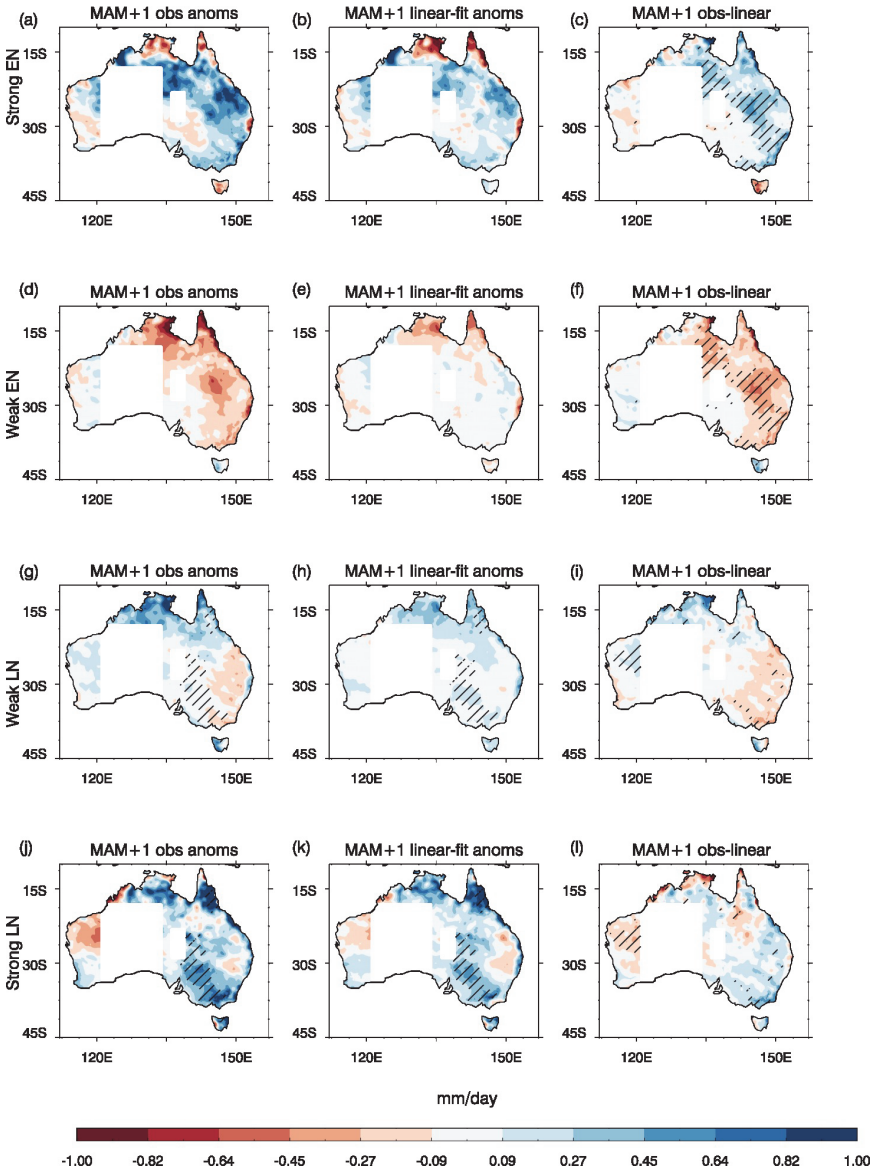

Figure 8 As in Fig 6, but for MAM+1 (the MAM directly following the June-December used in the SOI average).

In summary, Figs 6-8 show that when considering EN and LN years separately, there are some regions in which there is a significant non-linear relationship between rainfall and SOI. Additionally, some regions such as the northern NT and QLD (SON), a significant overall EN/LN non-linearity exists also, as shown in Figs 3. This means that in these regions, although the overall rainfall does vary with SOI, a linear fit to the data provides a poor fit at both coarse (2 bins) and fine (5 bins) SOI resolutions.

4 Non-linearity in total seasonal precipitation and decomposition of daily rainfall distributions

Having established the limitations of assuming a linear model to fit the rainfall-SOI relationship for all years, as well as for EN and LN years separately, we now examine in detail the overall non-linearity in total precipitation. To keep the analysis concise and clear, we consider only the all-SOI non-linearity in this section. We quantify the non-linearity by calculating the difference between the linear regression slopes for EN and LN years, i.e. $\Delta s = S_{LN} - S_{EN}$.

We also decompose the daily rainfall distribution into two factors: the fraction of rainy days per season F_P, and the mean rainfall per day on days when the rainfall is non-zero, P_d. The mean rainfall for a given season, P, can therefore be given by

$$P = F_P \times P_d. \quad (1)$$

From Eq (1), if either F_P or P_d (or both) vary non-linearly with SOI, P will typically be non-linear. Similarly, if both F_P and P_d are linear then P would also be non-linear. In order to compare the relative contributions of F_P and P_d to the overall non-linearity in P, we calculate two diagnostics: i) $D_F = F_P \times \overline{P_d}$, and ii) $D_P = P_d \times \overline{F_P}$, where the overbar denotes an average over all SOI values. D_F therefore reflects the functional dependence of F_P on the SOI, while D_P reflects the functional dependence of P_d on the SOI.

Maps of the overall non-linearity $\Delta s(P)$ are shown in Figs 9a and 10a for SON and DJF. We do not consider MAM+1 henceforth due to the weak rainfall-SOI correlation during this season. Stippling occurs when the difference in slopes for EN and LN years are significant at the five per cent level, as in Figs 3-5. To clarify the nature of the non-linearities shown in Figs 3-5, we also focus on two individual locations: one in SON and one in DJF. These regions are chosen because they display significant non-linearities in P that are representative of non-linearities over broader regions in which they occur. For each location, we calculate several diagnostics over a 1˚x1˚ grid centred on the chosen coordinates. We sort the data into five SOI bins, as defined in the previous section, and calculate D_F, D_P, and the least-squares linear fit for the binned data.

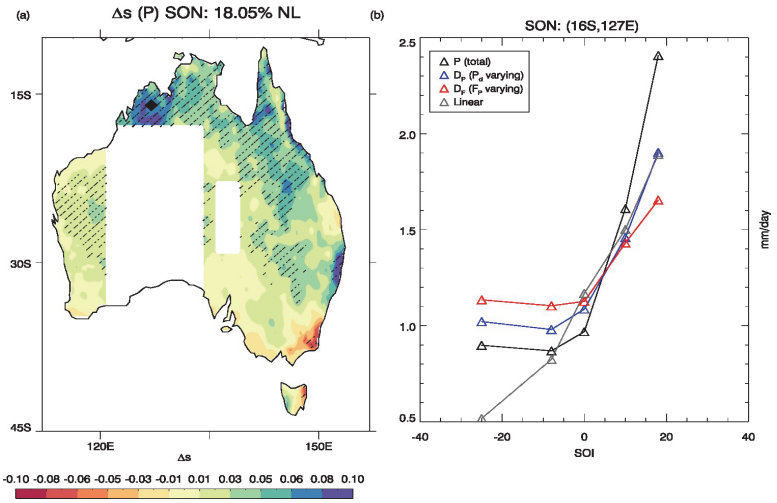

Figure 9 (a) Pattern of non-linearity, Δs(P) in average SON precipitation. Non-linearity is measured as the difference in linear regression coefficients between SOI > 0 years and SOI < 0. Stippling indicates five per cent significance. Black diamond denotes regions of interest. (b) Average SON precipitation P (black), DP (blue), and DF (red) for five SOI bins for the region of interest marked in panel (a). The least-squares linear fit for each region is shown in grey.

During SON, there are significant non-linearities over 18.05 per cent of the non-masked study area (Fig 9a). The largest non-linearities occur in northern Australia, with smaller, but significant, non-linearities over western WA. The region of interest chosen is in northwestern Australia (16˚S, 127˚E), and is marked by a diamond in Fig 9a. In this region, the mean seasonal precipitation is low during EN and neutral years, but increases sharply during LN years (Fig 9b). During EN and LN years, the observed rainfall (black line) is higher than expected from a linear fit (grey line). Both D_P (blue line) and D_F (red line) correlate well with P (> 0.85) in all regions of interest, with D_P correlating slightly better with P.

During DJF (Fig 10a), there are significant non-linearities over 12.75 per cent of the non-masked study area. The largest significant non-linearities are found over north and east Australia, with positive $\Delta s(P)$ indicating a stronger precipitation response during LN years. The region of interest (25˚S, 145˚E) lies in central QLD, and is marked by a diamond in Fig 10a. Fig 10b shows that in this region, the least rainfall occurs during neutral years, with a steep increase during both EN and LN years (black line). There is a large increase in rainfall between weak and strong EN/LN years, with strong EN years receiving almost as much rainfall as strong LN years. In this region, D_P is highly correlated with the total rainfall, whereas D_F is only weakly correlated.

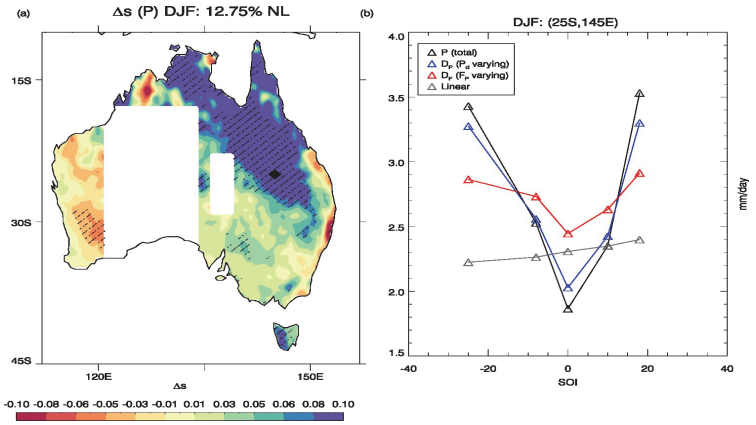

Figure 10 As per Fig 9, but for DJF.

For each location and each season, we calculated a linear fit to D_P and D_F separately, and multiplied the lines-of-best-fit, to see if the product of the linear components of D_P and D_F could reproduce some degree of the non-linearity in P (not shown). In each case, the product of the two lines-of-best-fit did not reproduce the non-linearity in P, indicating that the non-linearity in D_P and D_F is an essential factor in driving the non-linearity in the total precipitation.

4.1 Non-linearity in D_F and D_P

Fig 11 shows maps of the non-linearity in D_F, $\Delta s(D_F)$ (top row), and D_P, $\Delta s(D_P)$ (bottom row) for SON and DJF. Both D_F and D_P display significant non-linearities which contribute to the overall non-linearity in P. In general, both $\Delta s(D_F)$ and $\Delta s(D_P)$ are positive over northwest Australia during SON, and eastern Australia during DJF. While the patterns of both $\Delta s(D_F)$ and $\Delta s(D_P)$ are consistent with the non-linearity observed in the total precipitation, some differences between the two are apparent. The maps show that $\Delta s(D_F)$ is more uniform and is significant over larger areas than $\Delta s(D_P)$ in all seasons. In SON, both $\Delta s(D_P)$ and $\Delta s(D_F)$ have high spatial correlations with the overall non-linearity $\Delta s(P)$ ($r = 0.78$ and 0.62 respectively), whereas in DJF, the correlations are lower ($r = 0.19$ and 0.41 respectively).

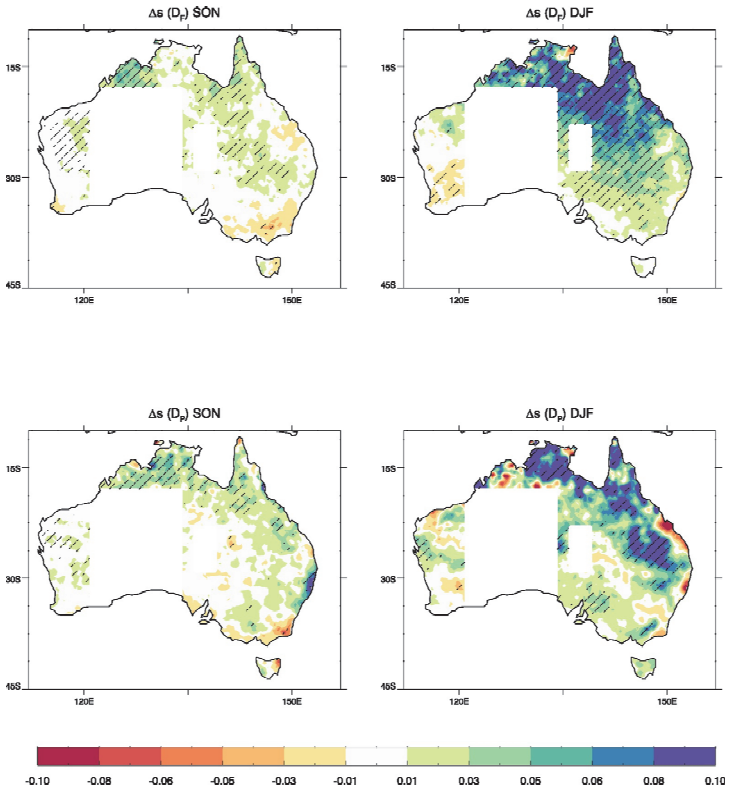

Figure 11 Top row: Non-linearity in, DF, the number of rainy days per season times the mean precipitation per rain day. Non-linearity is measured as the difference in linear regression coefficients between SOI > 0 years and SOI < 0 years for SON and DJF. Bottom row: Non-linearity in DP, the amount of rain per rain day times the mean fraction of rainy days per season. Stippling indicates five per cent significance.

The large degree of spatial and seasonal variability shown by $\Delta s(D_F)$ and $\Delta s(D_P)$ implies that the fraction of rainy days and amount of precipitation influence the overall rainfall-SOI non-linearity differently, depending on region and season.

5 Large-scale shifts

Over the Pacific, the asymmetric atmospheric response to ENSO SST anomalies results in a large-scale shift in precipitation patterns. The maximum precipitation over the equator shifts systematically from east to west as SST anomalies transition from EN to LN states (e.g., Power et al. 2013, Chung et al. 2014, Chung and Power 2014). Previous work has suggested that the non-linear precipitation response over Australia may also be due to a large-scale shift in precipitation patterns (e.g., Power et al. 2006, Cai et al. 2010).

To determine whether the precipitation patterns over and surrounding Australia shift systematically with the SOI, we calculate SON precipitation anomalies from 1979-2009 using GPCP satellite observations. Precipitation anomalies are presented in Fig 12 for (a) all SOI<0 years, (b) all SOI>0 years, (c) years with -5 < SOI < -10 (weak ENs), (d) years with 5 < SOI < 10 (weak LNs), (e) years with -10 < SOI < -15 (moderate ENs), (f) SOI > 10 (strong LNs), and (g) SOI < -15 (strong ENs). June-December average SOI values are used. Note that for the analysis of GPCP data in this section only, we use slightly different thresholds for the definition of strong EN and strong LN years due to the much smaller sample size. We do not produce a map for moderate LNs as there are no LN years with SOI > 15 from 1979-2009. In panel (h), we plot the sum of anomalies for all EN and all LN years. This provides an indication of EN/LN asymmetry, since the sum will be zero if the magnitudes are equal in magnitude, but opposite in sign.

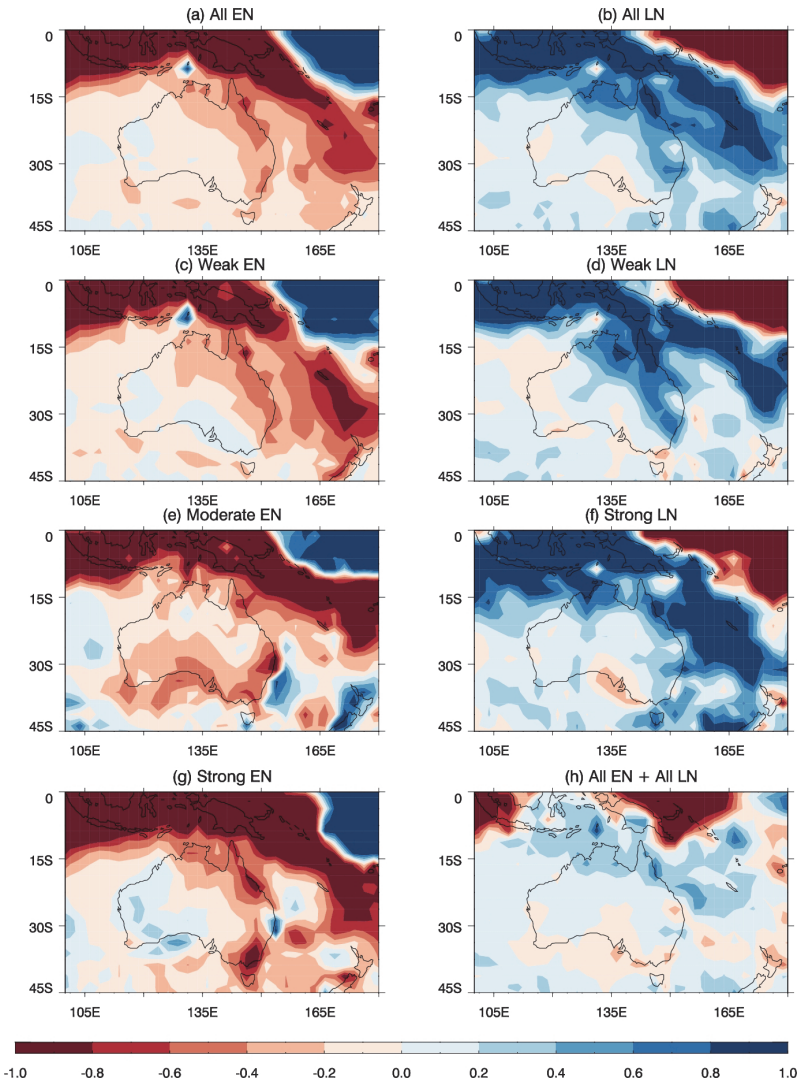

Figure 12 GPCP (1979-2009) SON precipitation anomalies for (a) all EN, (b) all LN, (c) weak EN, (d) weak LN, (e) moderate EN, (f) strong LN, and (g) strong EN years. Panel (h) shows the sum of anomalies for all EN and all LN years. Units are mm/day.

Over the equatorial Pacific (Fig 12a, c, e, g), there is a clear increase in precipitation over the central equatorial Pacific (165˚-180˚E) as the SOI decreases and EN events strengthen, as well as an eastward shift in the longitude of the maximum precipitation. This shift is accompanied by a drying over the maritime continent, which extends west into the Indian Ocean. While there is an overall drying during EN years over most of Australia, there is no systematic large-scale shift in the precipitation patterns. Figs 12c, 12e, and 12g show the varied precipitation response over Australia for weak, moderate, and strong EN years. Weak EN years produce a dry anomaly over northern and eastern Australia, while there is more drying over southern and southeastern Australia during moderate EN years. Strong EN years are associated with drying over northeast and southeast Australia, and are mildly wet in the southwest. Similarly, although there is an overall precipitation increase during LN years (Fig 12b), there is a lack of a systematic precipitation increase over a large part of Australia as LN strength increases. For example, some parts of eastern Australia experience more precipitation during weak LN years (Figs 12d and 12f) compared to strong LN years.

Comparing the anomalies for all EN (Fig 12a) and all LN years (Fig 12b), it is clear that while the precipitation anomalies over the region are similar (with opposite sign), they do not exactly mirror each other. For example, along the equator,

there is a westward shift of the zero-precipitation contour during LN years. During LN years, the South Pacific Convergence Zone (SPCZ) shifts southwards over northern Australia, whereas during EN years, the corresponding dry band does not extend as far south, consistent with earlier research (e.g., Salinger et al. 2014). To highlight the non-linearities, Fig 12(h) shows the sum of the anomalies for EN and LN years. As noted above, if the two were exactly equal in magnitude, but opposite in sign, they would cancel out. However, over northern Australia, the additional precipitation from LN years is evident.

From Fig 12, it is clear that while the precipitation non-linearities over the equatorial Pacific manifest as a shift of the maximum precipitation anomaly from west to east for weak to strong EN events, the precipitation anomalies over most of Australia do not systematically shift as the SOI changes. To further illustrate this point, Fig 13 shows precipitation profiles spanning 100˚E-180˚E, for four latitudes: i) 10˚S-0˚ (equatorial Pacific), ii) 20˚S-10˚S (northern Australia), iii) 30˚S-20˚S (central Australia), and (iv) 45˚S-30˚S (south Australia). Profiles are shown for weak, moderate, and strong EN events (left panels), and weak and strong LN events (right panels). Over the equatorial Pacific, the precipitation profiles are clearly stratified according to EN strength – from 100˚E-150˚E, the largest precipitation occurs during weak EN events, and the least during strong EN events. From 160˚E-180˚E, there is a clear eastward shift of the precipitation profiles as EN events go from weak to strong. The same can be seen during LN events – more precipitation occurs during strong LN events over the equatorial Pacific between 120˚E-160˚E. Over north, central, and south Australia however, there is no discernible pattern in the individual precipitation profiles for weak, moderate, and strong EN/LN events. However, comparing *all* EN years to *all* LN years (Fig 12 a, b), as expected the SPCZ extends southward during LN years (Salinger et al. 2014), generating additional precipitation over northern Australia (extending southward to approximately 20˚S). On average, there is more precipitation over northern Australia (10˚-20˚S) during LN years than EN years. Southward of 20˚S, the difference in precipitation profiles between EN and LN years is not as marked.

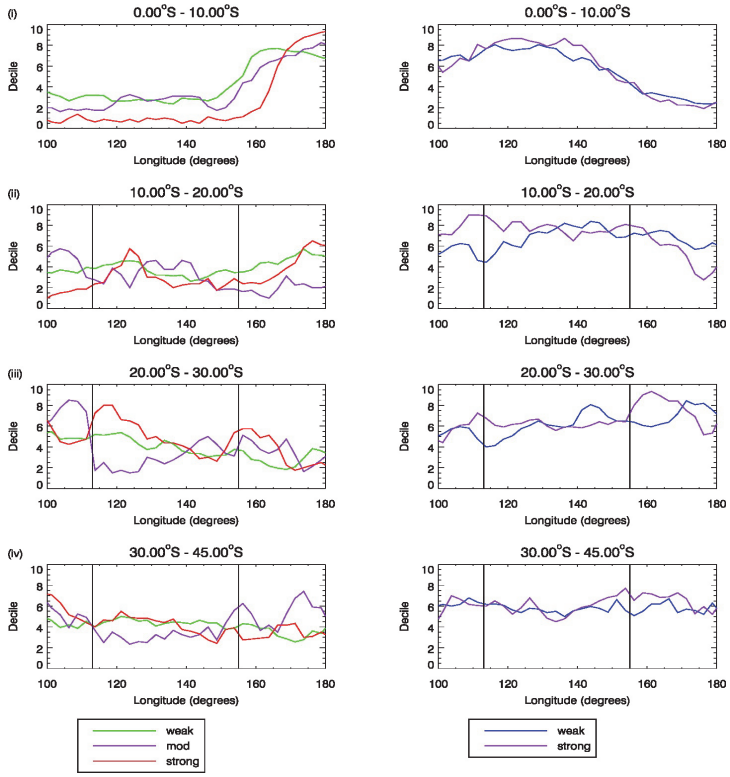

Figure 13 Observed GPCP (1979-2009) SON precipitation deciles along latitudinal cross sections spanning 100˚E-180˚E for weak, moderate, and strong EN years (left), and weak and strong LN years (right). From top to bottom, the latitudes used are i) 0-10˚S, ii) 10˚-20˚S (Northern Australia), iii) 20˚-30˚S, and iv) 30˚-45˚S. Vertical lines indicate the east- and west-most borders of the Australian continent.

One reason for this is that while precipitation over the Pacific is driven primarily by convection, over most of Australia there are many other factors influencing precipitation, (e.g., Risbey et al. 2009; Cai et al. 2010; Cai et al. 2011 Cai et al. 2012; Hendon et al. 2013; Braganza et al. 2015). Cai et al. (2012) attributed the LN-induced precipitation increase over northern Australia to convection anomalies, and EN-induced precipitation decrease over southern Australia to teleconnections with the tropical Indian Ocean.

6 Conclusion

We analysed seasonal means of daily Australian precipitation data from 1910-2012, to determine the nature of the seasonal rainfall-SOI relationship. While precipitation and SOI are highly correlated in large parts of the country in all seasons, a linear model fails to adequately describe the rainfall-SOI relationship in many regions during SON, DJF, and MAM+1.

In the literature (e.g., Cai et al. 2010; Cai et al. 2011; Cai et al. 2012), the degree of non-linearity in the rainfall-SOI relationship was obtained by fitting linear models to SOI<0 and SOI>0 years separately. Non-linearity arises because the two linear relationships – the one that holds for SOI<0 years and the one that holds for SOI>0 years, have statistically significant differences in their slopes. We therefore quantify non-linearity as the difference between S_{LN} and S_{EN}. Here S_{LN} is the regression coefficient between precipitation and the SOI (i.e. the slope of the line-of-best-fit) using data for SOI > 0 years only, and s_{EN} is the regression coefficient between precipitation and the SOI using data for SOI < 0 years only. In most cases, when comparing the data to the line-of-best-fit for all years, the non-linearity is caused by a larger-than-linear increase in precipitation during years with strong positive excursions of the SOI, and less-than-linear drying during years with strong negative excursions in the SOI. This is consistent with previous conclusions drawn on the basis of the relationship between all-Australian precipitation and the SOI (Power et al. 2006). This sort of non-linearity occurs during SON and DJF over the north and northeast of the country. During MAM+1, some non-linearity occurs over eastern Australia, but the correlation between rainfall and SOI is weak. During MAM-1 and JJA, the areal extent of non-linearity is not statistically significant (six per cent and three per cent of the total non-masked area respectively).

For SON, DJF, and MAM+1, we also tested the rainfall-SOI correlation and assumption of linearity within EN and LN years separately by dividing the data further into five equally spaced SOI bins and comparing the slopes of the lines-of-best-fit between the mean precipitation in each bin. In this case, non-linearity exists if the differences between the mean precipitation in each bin are significant (e.g., if the change between SOI≈0 and weakly negative SOI bins is significantly different from the change between weakly and strongly negative SOI bins). During SON and DJF, precipitation and SOI are significantly correlated over more of the country during LN years, and less so during EN years. In fact, during DJF, there is almost no significant correlation between precipitation and SOI anywhere in Australia during SOI<0 years. Significant non-linearities within EN and LN years also exist, although they cover a smaller area than the overall EN-LN non-linearity.

Some notable examples are as follows:

i) Southern QLD receives similarly large amounts of precipitation during both strong EN (SOI<-13) and strong LN (SOI>13) years (~3.5 mm/day) during DJF. During strong EN years, this is more than 1.5 times larger than expected from a linear precipitation response. This region also exhibits a significant non-linear relationship between precipitation and seasonal SOI within SOI<0 and SOI>0 years.

ii) During SON, the Kimberley region in northern Australia displays significant non-linearities. In this region, the average precipitation received during strong EN years is approximately 0.9 mm/day (double the amount predicted by a linear fit) and the precipitation received during strong LN years exceeds 2 mm/day, 25 per cent more than predicted by a linear fit to all years.

The total seasonal precipitation can be described as a product of the fraction of rainy days (F_D) and the amount of rain on rainy days (P_d). While it is clear that any non-linearity in F_D or P_D will typically contribute to non-linearity in P, we note also that even if both F_D and P_d are linear functions of SOI, their product can be non-linear. However, plotting the total precipitation P, D_F, and D_P versus SOI for several locations shows the non-linearity in the P-SOI relationship is a result of non-linearity in both F_D and P_d. Overall, however, there is a slightly higher correlation between P and P_d.

We investigated large-scale horizontal shifts in precipitation patterns over and around Australia as a possible explanation for the non-linearity. Over the equatorial Pacific, the convection-driven precipitation has a clear non-linear relationship with SOI – the amount of precipitation over the equatorial Pacific increases non-linearly, and the maximum precipitation anomaly shifts eastward as SOI decreases. As noted by previous work (e.g., Cai et al. 2010; Cai et al. 2012) when looking at all EN and all LN years on average, LN years bring about more precipitation over northern Australia due to the westward displacement of the precipitation anomalies over the tropical Pacific. Southward of approximately 10˚S, however, we find no distinct systematic shifts in the precipitation patterns for weak, moderate, and strong EN events, or for weak and strong LN events.

One caveat to the analysis presented is the issue of sample size, in which small sample sizes may be influenced by an extreme response in a particular year. In the 102 years considered in this study, there are 20 weak EN years, 22 weak LN years, 6 strong EN years, and 7 strong LN years. However, from Fig 1, it is evident that the non-linear rainfall-SOI relationship is robust and not skewed by any one particular year. For example, the years which received the largest amount of SON/DJF rainfall coincided with strong LN years, and the years which received the least amount of SON/MAM+1 rainfall did not coincide with strong EN years. Additionally, we note that while ENSO is the major driver of Australian precipitation, there are many other processes which influence the precipitation in a particular region, during a particular season (e.g., Wang and Hendon 2007; Lim et al. 2009; Taschetto and England 2009; Cai et al. 2010; Cai et al. 2011; Cai et al. 2012; Hendon et al. 2013; King et al. 2013; Braganza et al. 2015). Of particular interest would be the question of how multi-decadal processes such as the Interdecadal Pacific Oscillation (IPO) influence the non-linear ENSO-driven precipitation response over Australia we have identified. Previous studies have identified a stronger correlation between negative (positive) SOI and Australian rainfall during positive (negative) phases of the IPO (Power et al. 1999; Arblaster et al. 2002). However, this apparent modulation may be due to the non-linear ENSO-rainfall relationship over Australia (Power et al. 2006; Westra et al. 2015).

Acknowledgments

The authors would like to thank Eunpa Lim, Guomin Wang, Peter May and anonymous reviewers for constructive comments that have improved the manuscript. This work was supported by the by the Australian Government Department of the Environment, the Bureau of Meteorology and CSIRO through the Australian Climate Change Science Program (ACCSP). The authors would like to thank Lynda Chambers and Catherine Ganter for helpful discussions.

References

Adler, R.F., Huffman, G.J., Chang, A., Ferraro, R., Xie, P., Janowiak, J., Rudolf, B., Schneider, U., Curtis, S., Bolvin, D., Gruber, A., Susskind, J., Arkin, P. and Nelkin E. 2003. The Version 2 Global Precipitation Climatology Project (GPCP) Monthly Precipitation Analysis (1979-Present). *J. Hydrometeor.* 4:1147-1167.

Allan R. 1988. El Niño-Southern Oscillation influences in the Australasian region. *Prog. Phys. Geogr.* 12:313-348

Arblaster J.M., Meehl G. A. and Moore A. M. 2002. Interdecadal Modulation of Australian Rainfall. *Climate Dynamics* 18:519-531. doi: 10.1007/s00382-001-0191-y

Braganza, K., Murphy, B., Timbal, B., Hope, P., Dowdy, A., Hennessy, K., Bhend J. and Kirono, D. 2015. Chapter 4 – Understanding Australian climate. In: *CSIRO and Bureau of Meteorology 2015, Climate Change in Australia Information for Australia's Natural Resource Management Regions: Technical Report*, CSIRO and Bureau of Meteorology, Australia, 216 pp.

Cai, W., van Rensch, P., Cowan ,T. and Sullivan, A. 2010. Asymmetry in ENSO Teleconnection with Regional Rainfall, Its Multidecadal Variability, and Impact. *J Climate,* 23:4944-4955

Cai, W., van Rensch, P., Cowan, T. and Hendon, H.H. 2011. Teleconnection Pathways of ENSO and the IOD and the Mechanisms for Impacts on Australian Rainfall. *J Climate,* 24:3910-3923

Cai, W., van Rensch, P. and Cowan, T. 2012. An Asymmetry in the IOD and ENSO Teleconnection Pathway and Its Impact on Australian Climate. *J Climate,* 25:6318-6329

Callaghan, J. and Power, S.B. 2014. Major coastal flooding in southeastern Australia 1860-2012, associated deaths and weather systems. *Aust. Meterol. Oceanogr. J.* 64:183-213.

Chung, C.T.Y. , Power, S.B. , Arblaster, J.M., Rashid, H.A. and Roff, G.L. 2014. Nonlinear precipitation response to El Niño and global warming in the Indo-Pacific. *Climate Dynamics*, 42:1837-1856

Chung, C.T.Y. and Power, S.B. 2014. Precipitation response to La Niña and global warming in the Indo-Pacific. *Climate Dynamics,* 43:3293-3307. DOI: 10.1007/s00382-014-2105-9

Hendon, H.H., Lim, E.-P., Arblaster, J.M. and Anderson, D.L.T. 2013. Causes and predictability of the record wet spring over Australia in 2010. *Climate Dynamics,* 42:1155–1174, doi:10.1007/s00382-013-1700-5.

Hoerling M.P., Kumar, A. and Zhong, M. 1997. El Niño, La Niña, and the non-linearity of their teleconnections. *J Climate,* 10:1769–1786

Hu, Z.Z. , Kumar, A., Jha, B., Wang, W., Huang, B. and Huang, B. 2012. An analysis of warm pool and cold tongue El Niños: air-sea coupling processes, global influences, and recent trends. *Climate Dynamics*, 38:2017-2035.

Jones, D.A., Wang, W. and Fawcett, R. 2009. High-quality spatial climate data-sets for Australia. *Aust Meteor. Oceanorgr. J.* 58:233-248

King, A.D., Alexander, L.V. and Donat, M.G. 2012. The efficacy of using gridded data to examine extreme rainfall characteristics: a case study for Australia. *International Journal of Climatology*, 33(10):2376-2387

King, A.D., Alexander, L.V. and Donat, M.G. 2013. Asymmetry in the response of eastern Australia extreme rainfall to low-frequency Pacific variability. *Geophys. Res. Lett*. 40, 2271-2277, doi:10.1002/grl.50427.

King, A.D., Donat M.G., Alexander L.V. and Karoly D.J. 2015. The ENSO-Australian rainfall teleconnection in reanalysis and CMIP5. *Climate Dynamics,* 44:2623-2635

Lim, E.-P., Hendon, H.H., Hudson, D., Wang, G. and Alves, O. 2009. Dynamical Forecast of Inter–El Niño Variations of Tropical SST and Australian Spring Rainfall. *Mon. Wea. Rev*. 137:3796–3810.

Livezey, R.E. and Chen, W.Y. 1983. Statistical Field Significance and its Determination by Monte Carlo Techniques. *Mon. Wea. Rev*. 111:46-59

McBride, J.L. and Nicholls, N. 1983. Seasonal relationships between Australian rainfall and The Southern Oscillation. *Mon. Wea. Rev*. 111:1998-2004.

Murphy, B.F., Power, S.B. and McGree, S. 2014. The Varied Impacts of El Niño–Southern Oscillation on Pacific Island Climates. *J. Climate*, 27:4015–4036.

Mullan, A.B. 1995. On the linearity and stability of Southern Oscillation-climate relationships for New Zealand. *Int. J. Climatol*., 15: 1365–1386. doi:10.1002/joc.3370151205

Nicholls, N., Drosdowsky, W. and Lavery, B. 1997. Australian rainfall variability and change. *Weather,* 52:66-71

Philander, S. 1990. El Niño, La Niña, and the Southern Oscillation. *Academic Press*

Power, S.B. and Mysak, L.A. 1992. On the interannual variability of Arctic Sea-level pressure and sea-ice drift. *Atmosphere-Ocean,* 30:551-575.

Power, S., Tseitkin, F., Torok, S., Lavery, B., Dahni, R. and McAvaney, B. 1998. Australian temperature, Australian rainfall and the Southern Oscillation, 1910-1992: coherent variability and recent changes. *Australian Meteorological Magazine,* 47: 85-101.

Power, S., Tseitkin, F., Mehta, V., Lavery, B., Torok, S. and Holbrook, N. 1999. Decadal climate variability in Australia during the twentieth century. *International Journal of Climatology,* 19: 169-184.

Power, S., Haylock, M., Colman, R. and Wang, X. 2006. The predictability of interdecadal changes in ENSO and ENSO teleconnections. *Journal of Climate*, 19:4755–4771

Power, S.B. and Smith, I.N. 2007. Weakening of the Walker Circulation and apparent dominance of El Niño both reach record levels, but has ENSO really changed? *Geophys. Res. Lett.*, 34, doi:10.129/2007/GL30854.

Power, S. B., Delage, F., Chung, C. T. Y., Kociuba, G. and Keay, K. 2013. Robust twenty-first century projections of El Niño and related precipitation variability. *Nature,* 502:541-545 doi:10.1038/nature12580.

Power, S., Folland, C., Colman, A. and Mehta, V. 1999. Inter-decadal modulation of the impact of ENSO on Australia. *Climate Dynamics*,15, 319-324.

Risbey, J.S., Pook, M.J., Mcintosh, P.C., Wheeler, M.C. and Hendon, H.H. 2009. On the Remote Drivers of Rainfall Variability in Australia. *Monthly Weather Review*, 137:3233-3253

Ropelewski, C.F. and Halpert, M.S. 1987. Global and regional scale precipitation patterns associated with the El Niño/Southern Oscillation. *Monthly Weather Review*, 115(8):1606-1626.

Saji, N.H., Goswami, B.N., Vinayachandran, P.N. and Yamagata, T. 1999. A dipole mode in the tropical Indian Ocean. *Nature*, 401:360-363

Salinger, J., McGree, S., Beucher, F., Power, S. and F. Delage. 2014. A new index for movements in the South Pacific Convergence Zone, *Climate Dynamics*, 43:881-892, doi: 10.1007/s00382-013-2035-y.

Smith, I., Moise, A., Inape, K., Murphy, B., Colman, R., Power, S.B. and Chung, C.T.Y. 2013. ENSO-related rainfall changes over the New Guinea region. *Journal of Geophysical Research: Atmospheres*, 118:10556-10675.

Sun, X., Renard, B., Thyer, M., Westra, S. and Lang, M. 2015. A global analysis of the asymmetric effect of ENSO on extreme precipitation. *Journal of Hydrology*, 530:51-65

Taschetto, A.S. and England, M.H. 2009. El Niño Modoki Impacts on Australian Rainfall. *J. Climate,* 22:3167–3174, doi: http://dx.doi.org/10.1175/2008JCLI2589.1.

Wang, G. and Hendon, H.H. 2007. Sensitivity of Australian rainfall to inter-El Niño variations. *J. Climate,* 20:4211-4226.

Westra, S., Renard, B. and Thyer, M. 2015. The ENSO–Precipitation Teleconnection and Its Modulation by the Interdecadal Pacific Oscillation. *J. Climate*, 28: 4753-4773

7 Appendix

In 'Map significance and seasonal coverage of non-linearity', we applied a Monte Carlo technique (Livezey and Chen 1983; Power and Mysak 1992) to determine whether a statistically significant fraction of the country displayed non-linearity. To do this, 1000 random SOI values were generated and assigned to observed rainfall values. The difference between the EN and LN linear regression coefficients, Δs, was calculated at each non-masked grid point. For each trial, the total area covered by statistically significant non-linearity (i.e. where the EN and LN regression coefficients were significantly different according to a t-test) was calculated and compared to observations. For a given season, the non-linearity was deemed significant at the five per cent level if the total area covered by observed non-linearity was larger than the area covered by non-linearity from 95 per cent of the trials. Using this method, SON (18.05%), DJF (12.75%), and MAM+1 (10.7%) had statistically significant coverage, whereas MAM-1 (6.2%) and JJA (3.2%) did not.